Shock Interference Heating in Hypersonic Flows

FRANK D. HAINS*
Bell Aerospace, Division of Textron, Buffalo, N. Y.
AND
J. WAYNE KEYES†
NASA Langley Research Center, Hampton, Va.

A theoretical and experimental study is made of shock interference heating on a variety of basic body shapes and flow conditions. Measurements of pressure and heat transfer are obtained in four wind tunnels at NASA Langley Research Center. These data cover a Mach number range from 6 to 20, and specific heat ratios from 1.20 to 1.67. Peak heating measurements up to 17 times ordinary stagnation point rates and pressure peaks up to 8 times free-stream pitot pressure are recorded. Numerical results from computer codes developed for each of the six types of interference compare favorably with most of the experimental data. A theoretical parametric study determined the effects of Mach number, specific heat ratio, and impinging shock strength on amplification of pressure and heat transfer. The results of this study show that a knowledge of heating can be important for the design of hypersonic vehicles such as the space shuttle. The problem is intensified by the fact that the particular type of interference and the location of peak heating regions on the vehicle will vary along the flight trajectory.

Nomenclature

A = constant in Eq. (2)
c_p = specific heat
L_s = shock displacement length
L = length of wedge or fin
l_s = length of shear layer
M = Mach number
N = constant in Eqs. (1) and (2)
p = pressure
Q = heat-transfer rate
R_b = hemisphere nose radius
Re = Reynolds number
T = temperature
U = velocity
x = surface coordinate
X = x/L
α = angle of attack
β = shock angle
γ = specific heat ratio
δ = shear layer thickness at the wall
θ = body angle
θ_i = shock generator angle
θ_s = shear layer angle relative to body surface
λ = sweep angle
μ = viscosity
ρ = density

Subscripts
aw = adiabatic wall
ref = reference
pk = peak
t = total
w = wall
∞ = freestream

Received January 17, 1972; presented as Paper 72-78 at the AIAA 10th Aerospace Sciences Meeting; San Diego, Calif., January 17–19, 1972; revision received June 1, 1972. This study was performed at Bell Aerospace, Division of Textron, under NASA Contract 1-9606. The authors wish to thank D. Bushnell of NASA for aid in planning this study, and L. Weinstein and R. Watson of NASA for help in the wind-tunnel testing. In the early stages of this study, contributions were made by B. Edney and T. Bramlette. The computer programs were developed by J. Ives and P. Battaglia, and data reduction was handled by B. Okulewicz.

Index category: Supersonic and Hypersonic Flow.

* Principal Scientist, Advanced Technology Research; presently at Science Applications Inc., Arlington, Va.

† Aerospace Engineer, Hypersonic Vehicles Division.

Introduction

SHOCK interference heating is a serious problem for the space shuttle and other maneuverable re-entry vehicles. Extremely high heat-transfer rates, many times ordinary stagnation-point values, can occur in small regions on the vehicle surface. The peak heating is also accompanied by a pressure peak which further complicates the design of a practical thermal protection system.

Edney[1] has classified shock interference patterns into the six types as shown in Fig. 1. In the diagrams of each type, A is the impinging shock, B is the bow shock of the body, and C is the interaction region on the body surface where peak heating and pressure occur. Shock/boundary-layer interactions are found in types I, II, and V, and shear layer attachment is found in type III. Type VI interference is characterized by an expansion fan/boundary-layer interaction which tends to lower the heat transfer. The most severe form of interference is type IV which has a supersonic jet embedded in a subsonic region. The impingement of this jet on the body surface produces intense heating and pressure peaks.

Some typical values of peak heating amplification are also shown in Fig. 1. The quantity Q_{ref} is the stagnation-point heating without interference, but with the same freestream conditions. The regions where interference heating may be found on a mated space shuttle during ascent are also shown in Fig. 1.

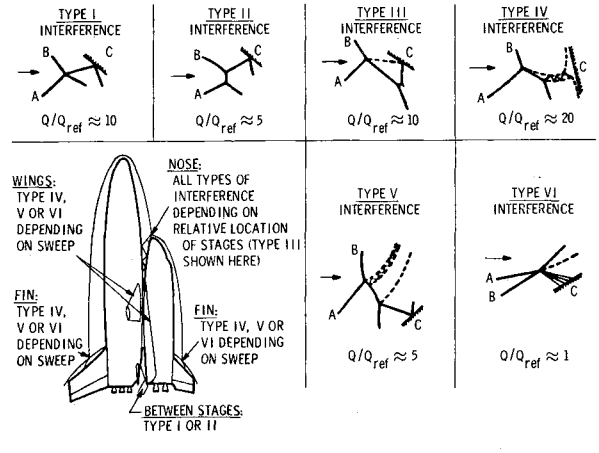

Fig. 1 The six types of shock interference.

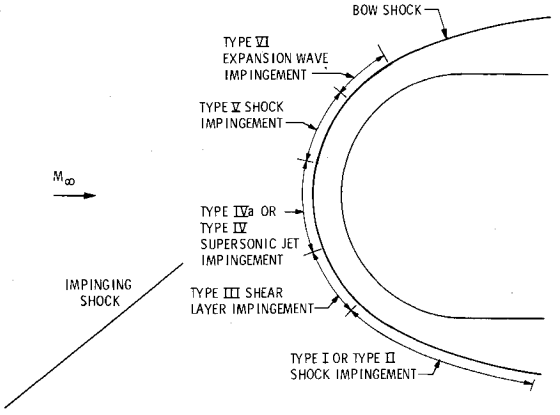

Fig. 2 Location of interference patterns on a hemisphere.

Interference heating can occur on the wing and tail surfaces, in the gap region between the vehicles, on the nose of the orbiter, and on deflected control flaps.

The position of ordinary stagnation points is usually known, but interference regions can move about. Figure 2 shows how the type of interference on a hemisphere is a function of the location of the impinging shock. In practice, the location of the peak heating regions will vary as the Mach number, freestream gas properties, angle of attack, etc., change along the flight path. In the present study, experimental measurements and photographs of the flowfield are used to locate and determine the type of interference.

Experimental Program

The objective of the experimental phase of this study is to determine the effects of Mach number, Reynolds number, ratio of specific heat, and position and strength of the impinging shock on the pressure and heat-transfer distribution on simple body shapes.

Tests were conducted in four facilities at the NASA Langley Research Center: 1) the 20-in. Hypersonic Air Tunnel (Mach 6), 2) the 22-in. Helium Tunnel (Mach 20), 3) the Mach 19 Hypersonic Nitrogen Tunnel, and 4) the Pilot Hypersonic CF_4 Tunnel. A plane impinging shock was produced by a variable-incidence wedge shock-generator. Four model configurations were used: a 2-in.-diam hemisphere, a 1-in.-diam hemisphere, a 1-in.-diam cylindrical leading-edge fin, and a plane wedge with 30° included angle. Pressure models were constructed of 347 stainless steel, and the heat-transfer models were made of a plastic silica base epoxy material. Some additional heat-transfer models were also made of 347 stainless steel to measure peak heating.

The method of testing was to first measure the pressure distribution on the model and at the same time photograph the shock patterns using schlieren, shadowgraph, or electron beam techniques. Conventional wind-tunnel techniques were used to measure the pressure. The shock generator angle remained fixed, the model position was varied in small increments so that the interference peaks could occur very near a pressure tap.

The heat-transfer tests were made using phase change coating technique.[2] As the coating on the model is heated, it melts at a known temperature and undergoes a visible phase change. Motion pictures of this process were used to obtain the time required for the phase change and the location of the melt lines. From this information, the heat transfer was obtained from a solution of the transient one-dimensional heat conduction equation. After the model was cooled to an ambient initial temperature and the coating was applied, it was exposed to the tunnel freestream flow, as quickly as possible. Several phase change coatings were used in order to obtain a heat-transfer distribution over the complete model.

Theoretical Models

A theoretical formulation was developed for each of the six types of interference. The ideal gas relations and inviscid flow assumptions were used to obtain the pressure distribution in the vicinity of the wall. The peak heat-transfer amplification that results from the shock/boundary-layer interaction in types I, II, and V was computed from the empirical correlation[3]

$$Q_{pk}/Q_{\text{ref}} = A[p_{pk}/p_{\text{ref}}]^N \tag{1}$$

The quantity p_{ref} is the value upstream of the shock/boundary-layer interaction and Q_{ref} was calculated from a reference temperature method[4] for the case of no interference. For laminar flow, the constant N is 1.29 and for turbulent flow is 0.85.

Type III interference is characterized by an attaching shear layer. The shear layer, represented by a dashed line in Fig. 1, reaches the wall at point C where a reflected shock is formed. Once the inviscid flow is obtained and the state of the shear layer is known,[5] the heat transfer can be calculated from a correlation given by Bushnell and Weinstein[6] for reattachment of separated boundary layers. The peak heat-transfer rate is

$$Q_{pk} = A\rho_w U c_p (T_{aw} - T_w)[\mu_w \sin\theta_s/\rho_w U\delta]^N \tag{2}$$

where and μ_w are based on conditions downstream of the reflected shock. For laminar flow the constants A and N are 0.19 and 0.5, respectively, and for turbulent flow they are 0.021 and 0.2, respectively. The shear layer thickness δ is given by the expressions

$$\text{laminar} \quad \delta = 5[\mu l_s/\rho U]^{0.5} \tag{3a}$$

$$\text{turbulent} \quad \delta = 0.123 l_s \tag{3b}$$

where ρ, μ, and U are based on conditions upstream of the reflected shock. Further details on the application of this type of correlation to shock interference heating may be found in Ref. 7.

The details of a type IV flow pattern are shown in Fig. 3 for a shear layer with downward deflection. Up to the beginning of ference pattern. The flow conditions and coordinates of the jet up to the jet bow shock were computes from the method of characteristics. The supersonic jet is made up of the triangular regions labeled 6–8 in Fig. 3. The actual number of regions and location of the jet bow shock will depend on the standoff distance of the entire configuration. The jet stagnation pressure and hence the heat transfer will depend on conditions upstream of the jet bow shock. In the present study, peaks were calculated for normal impingement of the jet and location of the jet bow shock in either regions 7 or 8. Peak heating is assumed to be analogous to the stagnation heating on a blunt body submerged in a supersonic flowfield of the width of the jet. Jet stagnation

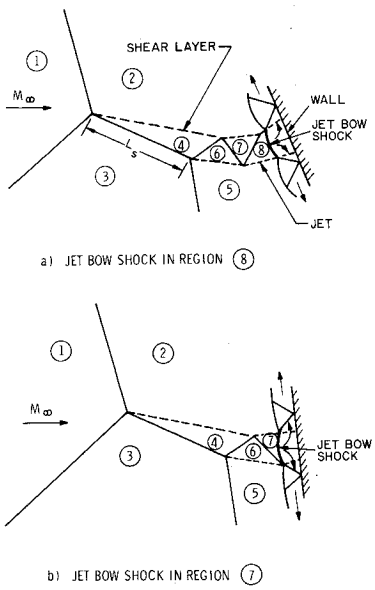

Fig. 3 Type IV interference patterns.

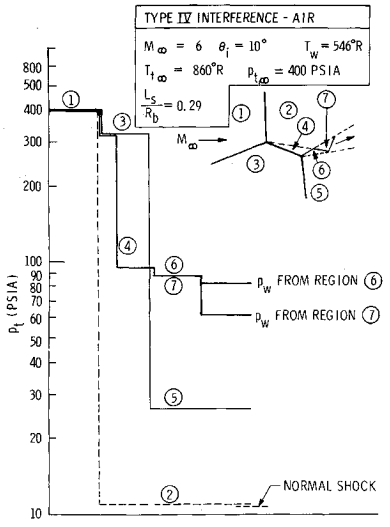

Fig. 4 Total pressure distribution for type IV interference.

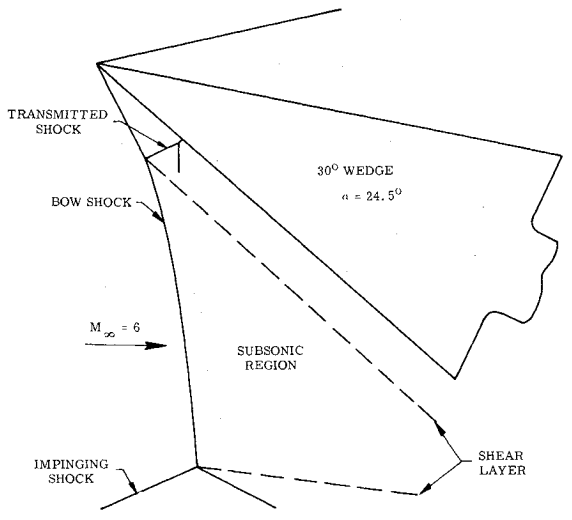

Fig. 6 Flowfield for type II interference on a wedge in air.

heating was obtained using the method of Ref. 8 and the velocity gradient expression of Ref. 9. The body radius used for the velocity gradient was obtained from the ratio of jet bow shock standoff distance to the jet width from flow pictures, the calculated jet widths, and the correlation of standoff distance to body radius as a function of the inverse of the normal shock density ratios from Ref. 10.

Type IV interference acts like an efficient inlet in slowing down the flow. The distribution of stagnation pressure along streamlines that pass through the various regions is shown in Fig. 4 along with the normal shock value without interference. Because the flow in the jet is decelerated by several weak shocks before it reaches the jet bow shock, the total pressure remains relatively high right up to the body surface. The wall pressure p_w is higher with the jet bow shock in region 6 because the total pressure in region 5 is higher than in region 2.

Type IV interference is sensitive to the value of the specific heat ratio γ. The ratio of the total pressure behind an oblique shock to that behind a normal shock increases significantly, especially at higher Mach numbers, with a decrease in γ. As shown in Fig. 5, when γ is reduced from 1.4 to 1.2, the calculated amplification in peak pressure is increased from 18.5 to 60 times the freestream pitot pressure. The main contribution for this increase is from a reduction in Q_{ref} rather than an increase in the peak values of p_w.

Type VI interference is characterized by an expansion fan/boundary-layer interaction which leads to a reduction in local heat transfer. Good correlations can probably be obtained from Eq. (1) if the proper values of the constant N is used. Additional data like that of Ref. 11 must be analyzed to determine if the values of these constants for shock waves can also be used for expansion waves.

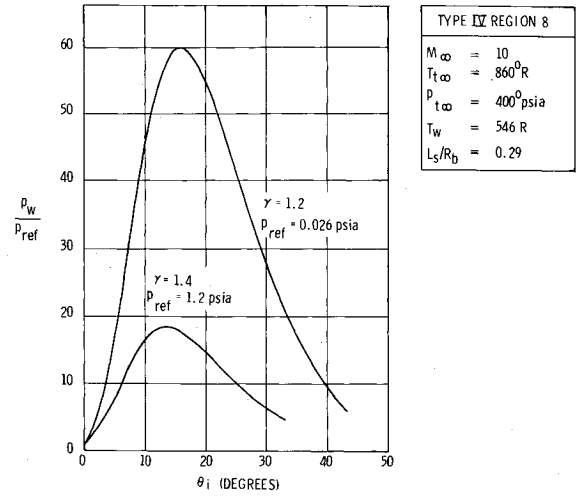

Fig. 5 Variation of wall pressure with γ for type IV interference.

Type II Interference on a Wedge

Figure 6 is a sketch made from a schlieren photograph of a type II interference pattern on the 30° wedge at an angle of attack of 24.5°. Although the impinging shock is far from the leading edge of the wedge, the interaction causes a kink in the bow shock close to the surface of the wedge where a triple shock and shear layer are produced. One shock strikes the wall and leads to the pressure rise shown in Fig. 7a. The associated heat transfer rise shown in Fig. 7b is about 15% higher than the value computed from the laminar form of Eq. (1).

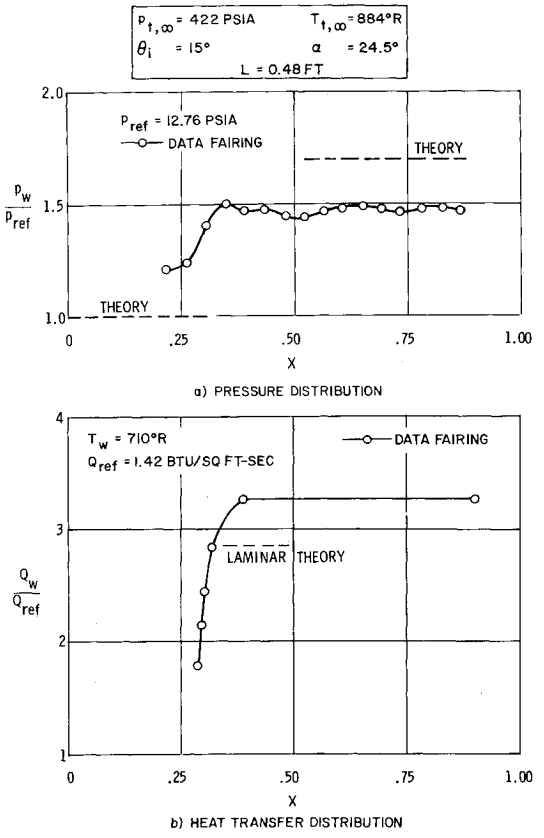

Fig. 7 Type II interference on a wedge in air. M_∞ = 6.0, Re_∞/ft = 7.8 × 10^6, γ = 1.40.

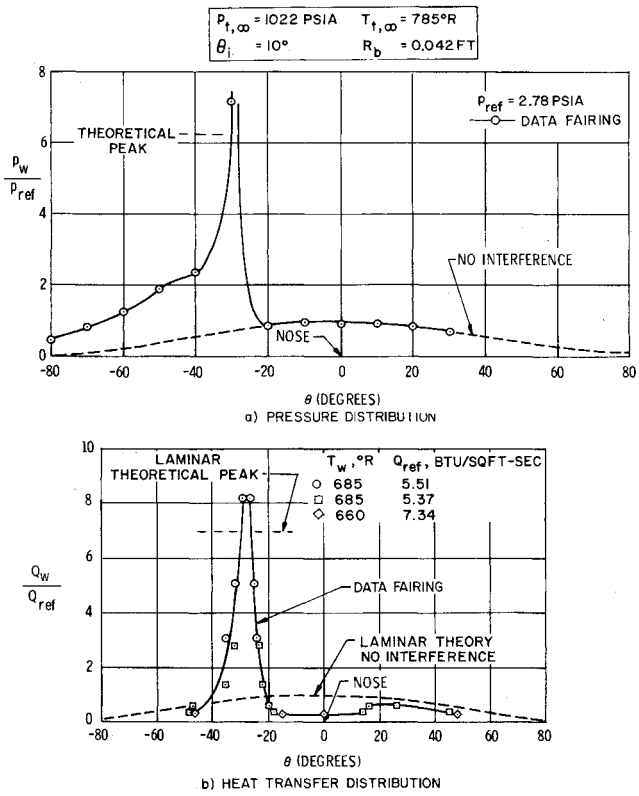

Fig. 8 Type III interference on a hemisphere in helium. $M_\infty = 20.2$, $Re/ft = 3.0 \times 10^6$, $\gamma = 1.67$.

Type III Interference on a Hemisphere

The type III interference pattern shown in Fig. 1 is characterized by an attaching shear layer. The results for a type III pattern on a hemisphere are shown in Fig. 8. The measured heat-transfer peak is eight times the stagnation-point rate without interference. In contrast to type IV interference no secondary peaks were produced. The theoretical peaks agree fairly well with the measurements, but some additional improvement may be achieved by accounting for the shear layer thickness in the inviscid model, and the higher values of θ_s encountered in the present case[7] as compared to those in Ref. 6.

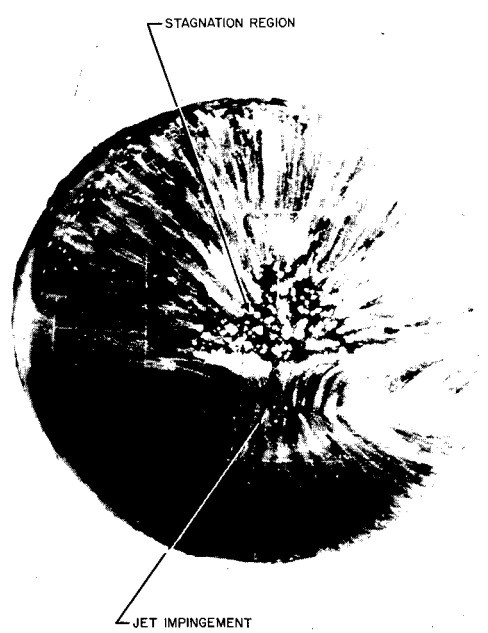

Fig. 9 Oil flow on a hemisphere with type IV interference in CF_4.

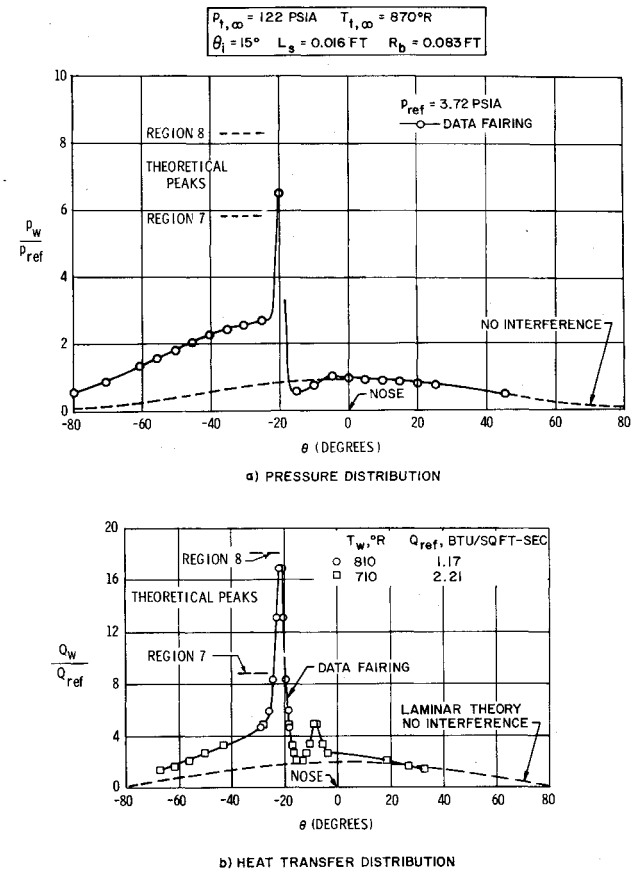

Fig. 10 Type IV interference on a hemisphere in air. $M_\infty = 6.0$, $Re_\infty/ft = 2.3 \times 10^6$, $\gamma = 1.40$.

Type IV Interference on a Hemisphere

Type IV interactions similar to those sketched in Fig. 3 were obtained on a 2-in. hemisphere in air at Mach 6. Oil flow tests were not made in the air tunnel, but results of a similar test in the CF_4 Tunnel are shown in Fig. 9. The impingement of the jet creates a horizontal stagnation line with flow moving away from the line in both directions. On the lower half in the vicinity of the vertical plane of symmetry, the assumption of planar flow appears to be valid. Further away from this plane, three-dimensional effects appear.

Returning to the air tests, the measured peak pressure shown in Fig. 10a lies between the calculations for regions 7 and 8. Because the peak encompasses a region of only about 3° on the body surface while the pressure taps are located at intervals of 5°, the maximum value may have been missed. The heat-transfer amplification rate of 17 agrees well with the calculated value with the jet bow shock in region 8 as shown in Fig. 10b.

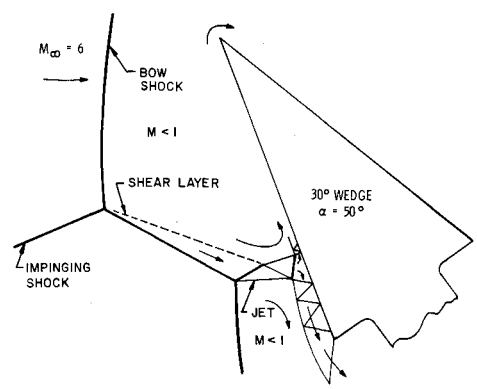

Fig. 11 Flowfield for type IV interference on a wedge in air.

Type IV Interference on a 30° Wedge

A flowfield diagram made from a schlieren picture of type IV interference on a 30° wedge at an angle of attack of 50° is shown in Fig. 11. The impingement of the jet is slightly oblique because a greater portion of the flow in the jet is turned toward the trailing edge of the wedge. The pressure peak shown in Fig. 12a is in good agreement with the theory for region 8 which predicts a peak of 8.4 times. The corresponding heat-transfer predictions shown in Fig. 12b for an axisymmetric stagnation point are lower than the measured peak.

Type V Interference on a Swept Fin

A type V pattern on a fin with 25° sweepback is shown in Fig. 13. This pattern has a detached supersonic jet and shear layer. The peak heating on the model surface is the result of a shock/boundary-layer interaction. The pressure distribution is shown in Fig. 14a. Because of the close proximity of the lower corner of the model, the pressure did not drop to the infinite fin value before rising to the peak. The highest measured value of pressure amplification of 2.4 times was much lower than the theoretical value of 4.95 times. This is probably a result of the pressure tap spacing.

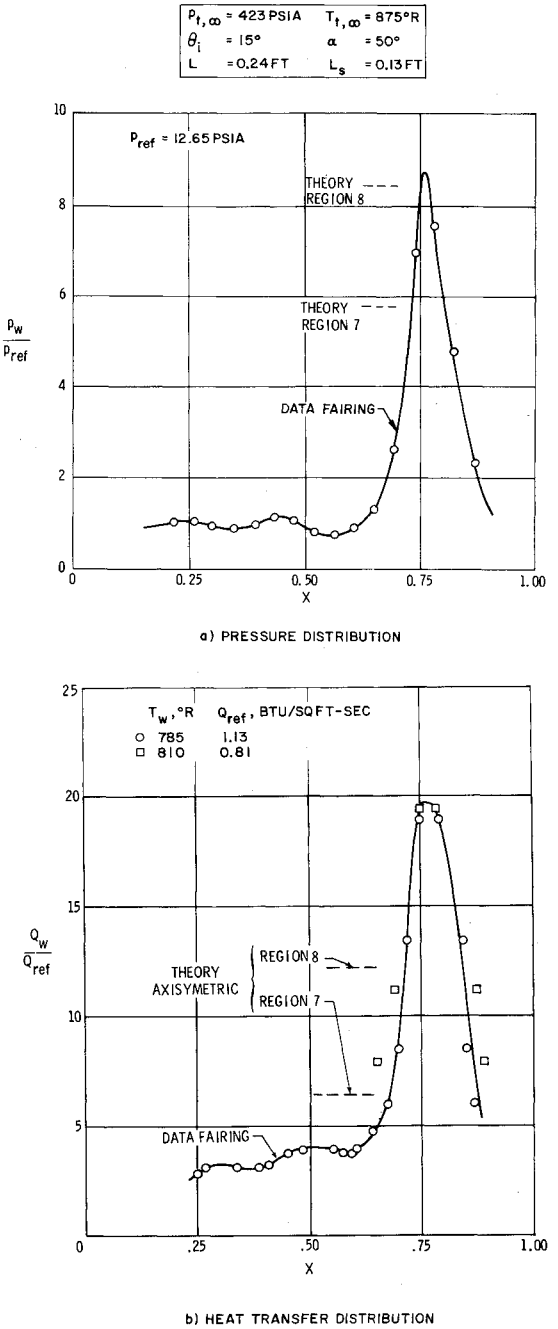

Fig. 12 Type IV interference on a wedge in air. $M_\infty = 6.0$, $Re_\infty/\text{ft} = 8.0 \times 10^6$, $\gamma = 1.40$.

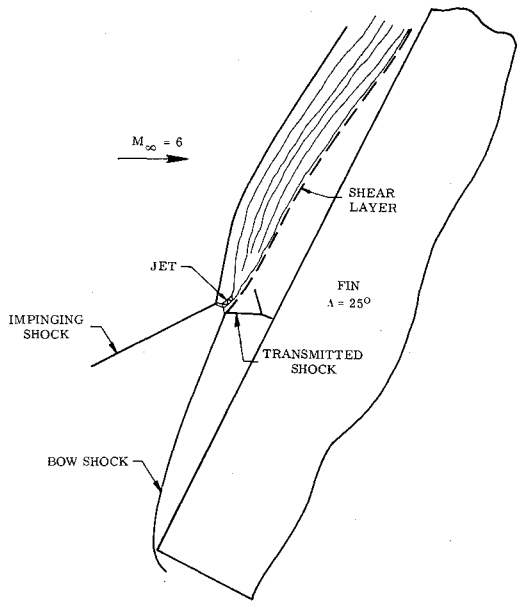

Fig. 13 Flowfield for a type V interference on a swept fin in air.

The heat-transfer distribution in Fig. 14b has a peak of 3.6 times which agrees well with the theoretical peak of 3.8 times. The angle β, which represents the inclination of the lower bow shock just below the interaction, was measured from the schlieren photograph corresponding to Fig. 13. The angle θ is the complement of the sweep angle, which in this case should be 65°. The value of 58° used in the calculation of the theoretical peak is the maximum allowable value of θ for a regular shock reflection at the wall. The secondary peak at $X = 0.62$ is caused by the thinning of the boundary layer by the grazing jet and shear layer.

Shock Interference Heating on the Space Shuttle

Shock interference heating is a serious problem for hypersonic vehicles like the space shuttle. Unlike an ordinary stagnation point, the location of the region of peak heating is not well defined. Instead, the interaction region will move about on on the body. This is illustrated in Fig. 15 where interference effects during ascent of a mated shuttle configuration are shown. Initially, there will be little or no shock interference between the two fuselages. As the vehicle accelerates, type V or VI interference appears on the upper surface of the orbiter. Heat-transfer rates up to 5 times stagnation values can be expected. With further increase in Mach number the interaction moves downward on the nose of the orbiter and type IV and III patterns will develop. Here, the largest heat-transfer rates will develop. Although amplification rates of about 20 times can be expected, it is not known at present whether significantly higher rates will be obtained if real gas effects are taken into account. A further increase in Mach number leads to a type II, and finally to a type I pattern. The bow shocks can reflect back and forth several times in the gap region between the vehicles to produce hot spots over an extended region on both fuselages.

Because of the importance of the trajectory on heat transfer, a calculation of type IV interference with $\gamma = 1.4$ was made along a typical space shuttle flight path during ascent. Freestream properties from atmospheric tables were used to an altitude of 250,000 ft. According to the results shown in Fig. 16, type IV interference could not develop below an altitude of 125,000 ft. The peak heat-transfer amplification can attain the value of

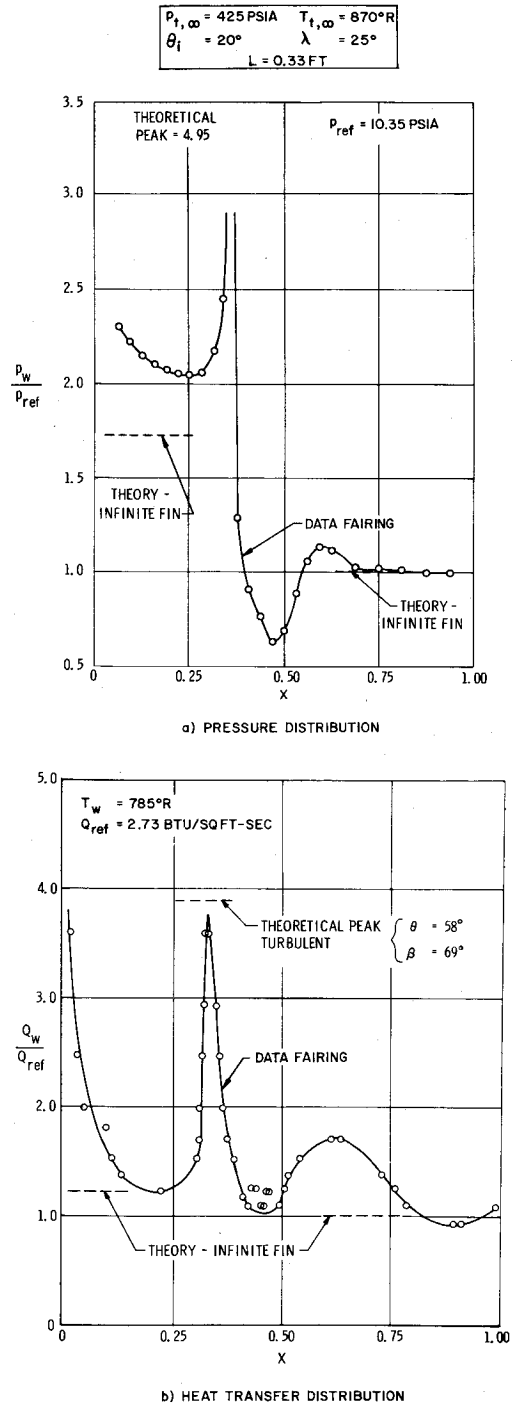

Fig. 14 Type V interference on a swept fin in air. $M_\infty = 6.0$, $Re_\infty/\text{ft} = 7.9 \times 10^6$, $\gamma = 1.40$.

37 times the ordinary stagnation-point rate if the jet bow stock is located in region 8. Even if the shock is located in region 7, an amplification rate of almost 20 times can be expected.

Conclusions

A theoretical and experimental study was made of shock interference heating effects in hypersonic flows. Interaction of a plane impinging shock wave with the bow wave generated by simple body shapes was considered. Of the six types of interference, type IV interference, which resulted in the impingement of a supersonic jet, is the most severe. In the present tests, heat-transfer amplification peaks of up to 17 times ordinary stagnation-point values and pressure amplification peaks of up to

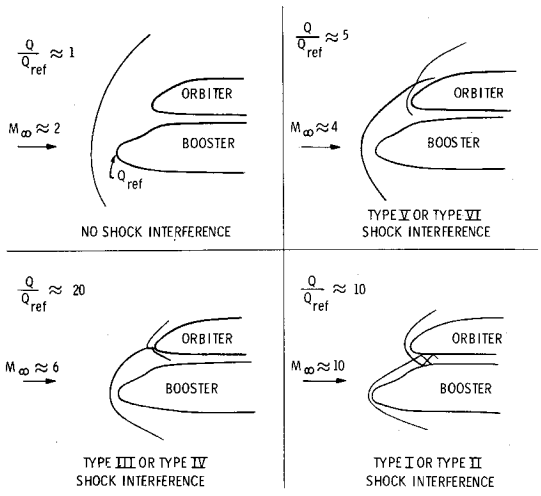

Fig. 15 Shock interference patterns on a space shuttle during ascent.

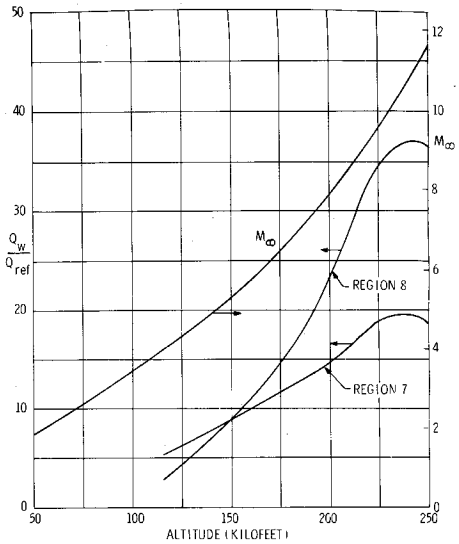

Fig. 16 Peak heat-transfer amplification for type IV interference on a typical space shuttle ascent trajectory ($\gamma = 1.40$).

8 times were measured in the vertical plane of symmetry. The results for type III interference, which leads to the attachment of a shear layer, is somewhat less severe than type IV. Measured values of pressure amplification of 4.2 times and heat-transfer amplification of 14 times were obtained. Maximum heat-transfer for a type V pattern on a 25° swept fin was 3.6 times the stagnation line value when there is no interference.

The computer codes based on ideal gas relations gave results that correlate well with the experimental data for gases of different specific heat ratio when real gas effects are not important. The theoretical model for type IV interference developed in this study shows that the magnitude of peak heating is very sensitive to the standoff distance of the entire shock pattern.

This study shows that shock interference heating can be one of the major problems of atmospheric flight at hypsrsonic speeds. Additional research is needed to fully understand the characteristics of these interactions so that engineers can design vehicles where these effects are avoided or at least kept to a minimum.

References

[1] Edney, B. E., "Anonalous Heat Transfer and Pressure Distributions on Blunt Bodies at Hypersonic Speeds in the Presence of an Impinging Shock," FFA Rept. 115, Feb. 1968, The Aeronautical Research Inst. of Sweden, Stockholm, Sweden.

[2] Jones, R. A. and Hunt, J. L., "Use of Fusible Temperature Indicators for Obtaining Quantitative Aerodynamic Heat-Transfer Data," TR R-230, Feb. 1966, NASA.

[3] Markarian, C. F., "Heat Transfer in Shock Wave-Boundary Layer Interaction Regions," NWC-TP-4485, Nov. 1968, Naval Weapons Center, China Lake, Calif.; also M.S. thesis, 1967, Univ. of California at Los Angeles, Los Angeles, Calif.

[4] Harms, R. J. et al., "A Manual for Determining Aerodynamic Heating of High-Speed Aircraft, Vol. I," Rept. 7006-3352-001, June 1959, Bell Aircraft Co., Buffalo, N. Y.

[5] Birch, S. F. and Keyes, J. W., "Transition in Compressible Free Shear Layers," *Journal of Spacecraft and Rockets*, Vol. 9, No. 8, Aug. 1972, pp. 623–624.

[6] Bushnell, D. M. and Weinstein, L. M., "Correlation of Peak Heating for Reattachment of Separated Flows," *Journal of Spacecraft and Rockets*, Vol. 5, No. 8, Aug. 1968, pp. 1111–1112.

[7] Keyes, J. W. and Morris, D. J., "Correlations of Peak Heating in Shock Interference Regions at Hypersonic Speeds," *Journal of Spacecraft and Rockets*, Vol. 9, No. 8, Aug. 1972, pp. 621–623.

[8] Fay, J. W. and Riddell, F. R., "Theory of Stagnation Point Heat Transfer in Dissociated Air," *Journal of the Aerospace Sciences*, Vol. 25, No. 2, Feb. 1958, pp. 73–85.

[9] Lees, L., "Laminar Heat Transfer over Blunt-Nosed Bodies at Hypersonic Speeds," *Jet Propulsion*, Vol. 26, No. 4, April 1956, pp. 259–269.

[10] Van Dyke, M. D. and Gordon, H. D., "Supersonic Flowpast a Family of Blunt Axisymmetric Bodies," TR R-1, 1959, NASA.

[11] Back, L. H. and Cuffel, R. F., "Changes in Heat Transfer from Turbulent Boundary Layers Interacting with Shock Waves and Expansion Waves," *AIAA Journal*, Vol. 8, No. 10, Oct. 1970, pp. 1871–1873.

NOVEMBER 1972 AIAA JOURNAL VOL. 10, NO. 11

Calculation of Compressible Turbulent Boundary Layers with Roughness and Heat Transfer

F. A. DVORAK*
The Boeing Company, Seattle, Wash.

A skin-friction law developed for incompressible turbulent boundary layers on rough surfaces in pressure gradient is extended to compressible flow by employing a procedure used previously by Spalding and Chi for smooth surfaces. The resulting equations coupled with the compressible momentum and entrainment integral equations provide a calculation method for predicting the growth of the compressible turbulent boundary layer over rough surfaces. Comparisons of the calculation method with a limited amount of experimental data indicate satisfactory agreement.

Nomenclature

$A\ B$ = constant in law of the wall
$C_0\ C_1\ C_2\ C_3$ = constants in polynomial [Eq. (A3)]
f = denoting functional dependence
G = pressure gradient parameter
k = roughness height
k_s = equivalent sand roughness
L = spacing between roughness elements (Fig. 9)
r, R = radius
S = length of roughness element (Fig. 9)
T = temperature
x, y = rectangular coordinates along and normal to the surface
U = local velocity outside boundary layer
U_∞ = undisturbed freestream velocity
U_τ = friction velocity
τ = shear stress
τ_w = local wall shear stress
δ = boundary-layer thickness
δ^* = displacement thickness $\int_0^y \left(1 - \frac{\rho u}{\rho_1 U}\right) dy$
θ = momentum thickness $\int_0^y \frac{\rho u}{\rho_1 U}\left(1 - \frac{u}{U}\right) dy$
ν = kinematic viscosity
ρ = density
c_f = local skin-friction coefficient $\tau_w/\frac{1}{2}\rho_1 U^2$
H = shape factor δ^*/θ
$\bar{H}$ = shape factor $\int_0^y \frac{\rho}{\rho_1}\left(1 - \frac{u}{U}\right) dy/\theta$
H_1 = shape factor $(\delta - \delta^*)/\theta$
λ = roughness density L/S
M = Mach number
R_C = chord Reynolds number Uc/ν
R_θ = momentum thickness Reynolds number $U\theta/\nu$
$U_\tau y/\nu$ = dimensionless distance normal to wall
$U_\tau k/\nu$ = dimensionless roughness height
$\Delta U_1/U_\tau$ = roughness contribution to law of wall
$\Delta U_2/U_\tau$ = pressure gradient contribution to velocity defect law

Subscripts

w = denoting wall conditions
0 = flat plate value
1 = local freestream value
r = recovery

Received December 20, 1971; revision received May 10, 1972.

Index categories: Boundary Layers and Convective Heat Transfer—Turbulent; Airplane and Component Aerodynamics; Rocket Vehicle Aerodynamics.

* Senior Engineer; presently Research Scientist, Flow Research Inc., Kent, Wash.

Introduction

A CALCULATION method previously developed by the author[1] for the prediction of incompressible turbulent boundary layers over rough surfaces in pressure gradient is extended herein to compressible flow with moderate heat transfer. Application of the method to the prediction of aircraft drag due to surface roughness should lead to improved predictions of aircraft performance. Other applications include the prediction of roughness effects on compressor, turbine or stator blades, and of the added drag due to acoustical treatment of gas turbine inlets.

In the present paper attention will be directed to a skin-friction law which includes the effects of heat transfer, surface roughness and pressure gradient and is useful in the Mach number range 0–5. When the skin-friction law is employed in conjunction with a turbulent boundary-layer calculation procedure, boundary-layer growth and friction drag may be predicted for two-dimensional or axisymmetric geometries. The following analysis is based upon earlier work by the author[1] and by Spalding and Chi.[2]

Skin-Friction Law in Incompressible Flow

The skin-friction law for incompressible flow is of the form

$$c_f = c_f(H, R_\theta, \Delta U_1/U_\tau) \tag{1}$$